N-type doping of SiC-passivated Ge by pulsed laser melting towards the development of interdigitated back contact thermophotovoltaic devices

A. Jiménez[1*], E. Napolitani[2,5], A. Datas[1*], I. Martín[3], G. López[3], M. Cabero[4], F. Sgarbossa[2,5], R. Milazzo[2], S. M. Carturan[2,5], D. de Salvador[2,5], I. Garcia[1], Y. K. Ryu[6], J. Martinez[6] and C. del Cañizo[1]

[1]Instituto de Energía Solar, Universidad Politécnica de Madrid, Spain, Av. Complutense s/n, 28040, Madrid, Spain
[2]Dipartamento di Fisica e Astronomia, Università degli Studi di Padova, via Marzolo 8, 35131 Padova, Italy
[3]Departament d'Enginyeria Electrònica, Universitat Politècnica de Catalunya, C/Jordi Girona 1-3, Mòdul C4, 08034 Barcelona, Spain
[4]Centro nacional de microscopía electrónica, Universidad Complutense de Madrid, Av. Complutense s/n, 28040 Ciudad Universitaria, Madrid
[5]INFN-LNL, viale dell'Università 2, 35020 Legnaro, Padova, Italy
[6] Instituto de Sistemas Optoelectrónicos y Microtecnología. Universidad Politécnica de Madrid. Avda Complutense 30, 28040, Spain.

*Corresponding authors: A. Jiménez (a.jimenez@ies.upm.es) and A. Datas (a.datas@upm.es)

1. ABSTRACT

In this article, a method for phosphorous (n-type) doping of germanium based on spin-on dopant sources and Pulsed Laser Melting (PLM) throughout an amorphous silicon carbide (a-Si_xC_{1-x}:H) layer, which provides both surface passivation and electrical isolation, has been demonstrated, paving the way towards the development of Ge-based interdigitated back contact thermophotovoltaic devices. This method offers simultaneous opening of the a-Si_xC_{1-x}:H layer and creation of a heavily doped region underneath without using photolithographic steps, eventually enabling a low-cost and scalable manufacturing process. This article focuses on the optimization of the n^+/p junction formation by studying the effect of different laser energy fluences and number of pulses on the diffusion profiles measured by secondary ion mass spectrometry, and on the electrical performance characterized by Van der Pauw-Hall technique. Additionally, the crystalline quality after PLM has been analyzed by Rutherford backscattering measurements in channeling conditions, high-resolution X-Ray diffraction and transmission electron microscopy. High level of donor activation (up to $1 \cdot 10^{19}$ cm^{-3}), low sheet resistance (≈50 Ω/□), and high mobility (275-700 $cm^2/V \cdot s$) have been obtained, with a weaker dependency of these parameters on the explored laser energy fluence range. A prototype diode has been developed demonstrating a rectifying behavior but with high saturation current densities. Point-like contact formation will be implemented in future works to reduce the laser irradiated area, and thus, improve the surface passivation and device characteristics.

2. INTRODUCTION

State of the art thermophotovoltaic (TPV) cells are based on a double-side contacted configuration, meaning that positive and negative electrodes are in opposite sides of the

device. However, this configuration has serious drawbacks concerning their integration in a TPV module. TPV modules must be densely populated with TPV cells, having a minimal space dedicated to the interconnection. Otherwise, a large fraction of thermal radiation would be lost in such inactive areas, significantly deteriorating the conversion efficiency. Several assembly concepts have been developed to manufacture dense-arrays using photovoltaic (PV) cells with a double-side contacted configuration [1]–[6], most of them involving relatively complex processes. These complexities could be avoided by using monolithic interconnected modules (MIM) [7] that have both electrodes in the front side. However, in this case complexity is transferred to the manufacturing of the MIM, which requires many photolithographic steps, and thus, could impact on the manufacturing yield. Furthermore, the active area of MIM is also reduced by the area dedicated to the front electrodes, including the sub-cell interconnections.

An alternative for simplifying dense-array module development are interdigitated back contact (IBC) TPV cells, which have both electrodes in the back side. This enables all interconnections to be made in the rear side, with a minimal separation between cells and a very high active area, due to the lack of shading elements in the front side. Solar PV Silicon based IBC devices have been widely developed for low [8]–[10] and high [11],[12] irradiance applications. However, to our knowledge, Ge-IBC cells have not been developed so far for TPV applications. *Nagashima et al*. proposed a conceptual Ge-based IBC TPV cell design with higher (theoretical) conversion efficiency (up to 25%) than conventional state of the art Ge-based TPV devices (16.5%) [13]-[14], but no experimental demonstrations have been conducted yet.

A key for the development of Ge-based IBC devices is the formation of high quality contacts that minimize surface recombination and enable selective carrier transport, along with ensuring the electrical insulation between electrodes [15]. A common strategy used in double-side contacted Ge TPV cells consist of forming an heterojunction by the deposition of wide band gap doped semiconductors, like amorphous silicon (a-Si:H) [16]–[21], or GaInP [22]–[25]. In this case, the combination of both field and chemical passivation have led to effective lifetimes in the order of 2100 µs in intrinsic c-Ge [14]. However, the formation of IBCs following this approach would be relatively complex, as different layers, having different dopants, should be deposited for each contact.

A simpler approach would be depositing a single electrically insulating passivating layer such as silicon nitride (SiN_x) [26] or a-Si_xC_{1-x}:H[14], followed by the local diffusion of dopants through this layer, using a laser source [27] (see fig. 1). This approach has been successfully used to form ohmic contacts to p-type c-Ge [21], [28]. But, to our knowledge, this strategy has not been yet demonstrated to form electron-selective contacts on Ge. This is the key missing step for the implementation of the full IBC TPV cell manufacturing process shown in fig. 1.

Therefore, the aim of this study is to explore the chemical, electrical and structural properties of electron selective contacts for c-Ge based on Pulsed Laser Melting (PLM)

of a phosphorus spin-on dopant (SoD) layer through the a-Si_xC_{1-x}:H passivation layer, similarly to the method proposed by *Wenham et al.* [29] implemented in Si-based devices. The results of this work could be valuable to guide the fabrication of highly efficient IBC TPV cells based on a simple and scalable manufacturing process.

3. MATERIALS AND METHODS

High purity Ge intrinsic wafers ($1 \cdot 10^{10}$ cm^{-3}) of 2 inches diameter with a thickness of 200 ± 20 µm and <100> oriented have been used as substrates. Figure 1 shows the process sequence for Ge doping based on laser irradiation of a solid dopant source on top of the passivating layer stack. The process starts with the surface preparation, which consists in a wet-chemical treatment in hydrochloric acid (HCl) 18% (v/v) for 3 min followed by an in-situ plasma cleaning under H_2 for 35 s, in order to effectively remove germanium oxide. Then, the deposition of a stack composed of intrinsic a-Si_xC_{1-x}:H (30 nm)/a-SiC:H (45 nm) layers (hereof called SiC stack) is carried out by using a direct Plasma-Enhanced Chemical Vapor Deposition (PECVD) reactor at 13.6 MHz. The effectiveness of the passivation stack is characterized by contactless photoconductance decay (PCD) measurements –adapted to Ge [30]- in samples with SiC stacksymmetrically deposited on both sides with effective carrier lifetime (τ_{eff}) in the order of 1 ms corresponding to effective surface recombination velocity below 15 cm/s. Afterwards, SoD P507 from Filmtronics® with a Phosphorus (P) concentration of $5 \cdot 10^{20}$ $atom \cdot cm^{-3}$ is deposited by spin-coating at 4500 rpm with a curing step at 200 °C to evaporate the remaining solvents as described more precisely in [31], which results in a film thickness of 220 ±10 nm. Subsequently, PLM is performed by a KrF excimer laser having a wavelength of 248 nm, 22 ns pulse duration with a top-hat distribution over an area of 5.1 x 5.1 mm^2 and a repetition frequency of 1 Hz. PLM allows to introduce P atoms contained in the SoD layer into Ge by surface melting and extremely short times solidification (in the order of hundreds of nanoseconds) of a shallow region of the irradiated sample, resulting in the creation of the n^+ region. In order to optimize the P surface concentration and the junction depth, the laser fluence is varied between 750 and 950 mJ/cm^2 and the number of pulses from 1 to 16. Prior to chemical and electrical characterization, the remaining SoD is removed with HF 10% (v/v) for 10min.

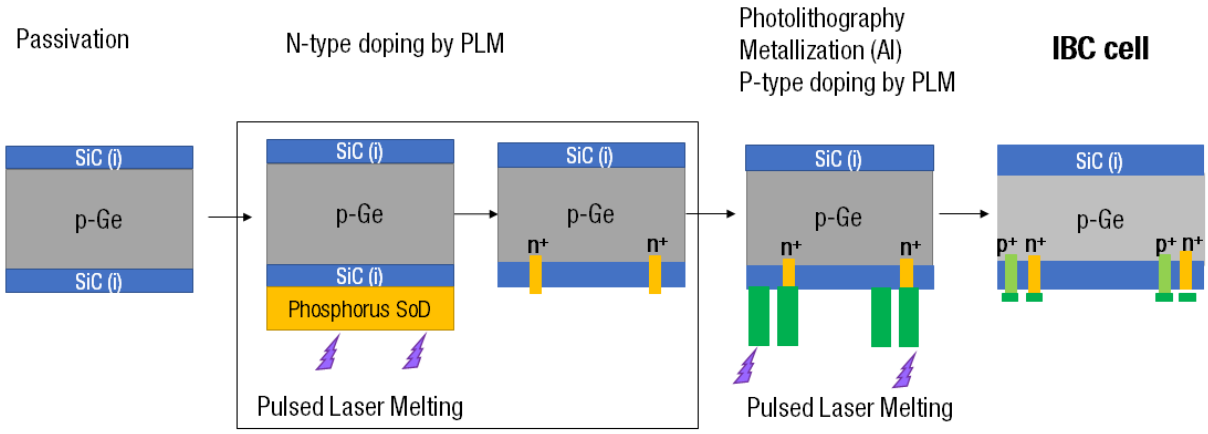

Fig.1. Process sequence for the creation of Ge-IBC cells by PLM through a dielectric stack

The P, Si, Ge and C chemical concentrations as a function of depth are measured by SIMS (Secondary Ion Mass Spectrometry) using a CAMECA instrument with a 5.5 keV Cs^+ ion primary beam while collecting $^{133}Cs_2{}^{12}C^+$, $^{133}Cs_2{}^{30}Si^+$, $^{133}Cs_2{}^{31}P^+$ and $^{133}Cs^{74}Ge^+$ secondary ions. The conditions for the primary ion beam, the energy and the secondary ion are carefully selected according to [32]-[33] as matrix effects are expected due to the presence of high concentration of Si in Ge as a result of the laser irradiation of the SiC stack. Additionally, the amount of Si incorporated in Ge and the crystalline quality of the samples is also estimated from Rutherford backscattering scattering measurements in <001> axial channeling conditions (c-RBS) by using a 2.0 MeV 4 He^+ beam and a scattering angle of 160°. In particular, the composition is determined by computer simulations using a layer by layer simulation program, based on Ziegler stopping power database [34]. The solid angle is calibrated by using a Ta on Si standard, with a known implanted Ta dose. Additionally, high-resolution X-ray diffraction (HR-XRD) measurements in the triple-axis configuration was performed using a Panalytical MRD X'PERT PRO diffractometer, equipped with a hybrid monochromator consisting of closely coupled X-Ray parabolic mirror and a Bartels 4 bounce Ge 220 monochromator, and transmission electron microscopy (TEM) have been done in order to corroborate the crystalline quality of the samples observed by c-RBS. TEM images are recorded using a JEOL JEM2100 with a CCD ORIUS SC1000 working at 200kV. Energy dispersive X-Ray spectroscopy (EDS) is performed using an aberration corrected scanning transmission electron microscope (STEM) model JEOL ARM200cF equipped with a spherical aberration corrector and an Oxford spectrometer, acquired at 200 kV.

The mobility and level of activation of P have been determined by Van der Pauw and Hall measurements (VdP-Hall). The electrically-active surface concentration has been determined by following the method described in [35]. To that end, we start from the SIMS profiles and calculate the maximum electrically-active P concentration (cm^{-3}) such that the integral of the P signal obtained from SIMS profile is equal to the electron areal density (cm^{-2}) measured by the Hall technique (assuming the Hall scattering factor γ_H=1). Finally, surface morphology is characterized by atomic force microscopy (AFM) (Nanoscope III, Bruker) (See Supplementary Material).

4.1. MATERIAL CHARACTERIZATION

Fig. 2 shows the P, Si, Ge and C chemical concentration as a function of depth as measured by SIMS of samples irradiated at 950 mJ/cm^2 and different number of pulses between 1 and 16. As it can be seen, not only P, but also Si and C atoms diffuse into Ge, and Ge diffuses towards the surface. The presence of Si and C in the deeper regions is explained by the melting of the SiC stack by laser irradiation above a certain energy fluence and diffusion of Si and C within the melt phase. Both Si and P diffuse very similarly. Their diffusion length is relatively narrow after the first pulse, but it becomes wider when the number of pulses increases. Besides, this broadening is unavoidably accompanied by a decrease of the surface concentration, as a result of the diffusion and redistribution of the atoms already incorporated during the first pulses. Contrarily, a very short diffusion length with a very high surface concentration is observed for the

case of C, independently of the number of pulses. This might be explained by its lower solubility in liquid Ge -in the order of 10^8-10^{10} cm^{-3} [36]- which could result in some C precipitation and segregation to the surface during cooldown or by the possible presence of small nanoclusters of C difficult to break owing to the high melting Tª of C (roughly x2.5 and x4 compared to Si and Ge, respectively) from which a lower diffusivity could be expected.

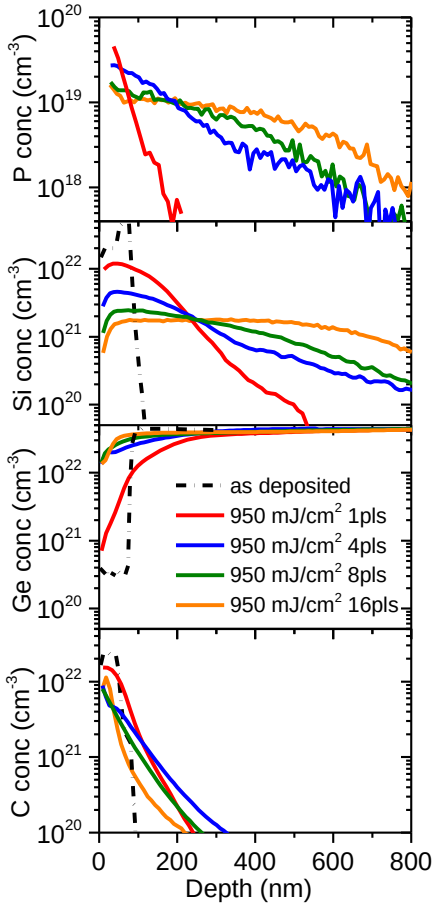

Fig.2 Chemical concentration profiles of P, Si, Ge and C for an energy fluence of 950 mJ/cm^2 and different number of pulses -pls in the graph- (1,4,8 and 16 pulses are represented by color lines red, blue, green and yellow, respectively). An as-deposited sample is also reported as a reference (black dash dot line).

The accuracy of the SIMS results is confirmed by the c-RBS measurements showed in Fig. 3, where the off-site Si dose (cm^{-2}) -calculated as the integral of the area under the element peak in c-RBS measurements-, shows a very good agreement with SIMS measurements (inset of Fig. 3) in the regime between 0 and 4 pulses, i.e. where the layer is highly disordered and all the Si atoms are off-site (see below). Thus, confirming that matrix effects are effectively prevented with the conditions judiciously used for the SIMS measurements.

Moreover, also the crystalline quality of the samples irradiated with laser can be assessed with the c-RBS measurements.

Fig. 3 shows the yield (total number of detected ions or counts) normalized to the total ion-beam charge as a function of energy (keV) for samples irradiated with a laser fluence of 950 mJ/cm^2 from 1 to 16 pulses. As it can be observed, a large peak at 1400-1600 keV corresponding to the Ge surface region and another one at 1100 keV corresponding to Si appear in the laser-irradiated samples up to 4 pulses, indicating that a surface layer highly defective, or even polycrystalline, is formed after PLM. We believe that an effective liquid phase epitaxial regrowth is hindered by the high Si concentration still present in these samples (above 10% as reported in Figure 2). The aforementioned peaks start to vanish in samples with over 8 pulses indicating that a huge improvement in Ge crystalline quality occurs as soon as the Si concentration is reduced (the Si concentration after 8 pulses is below 5% as reported in Figure 3).

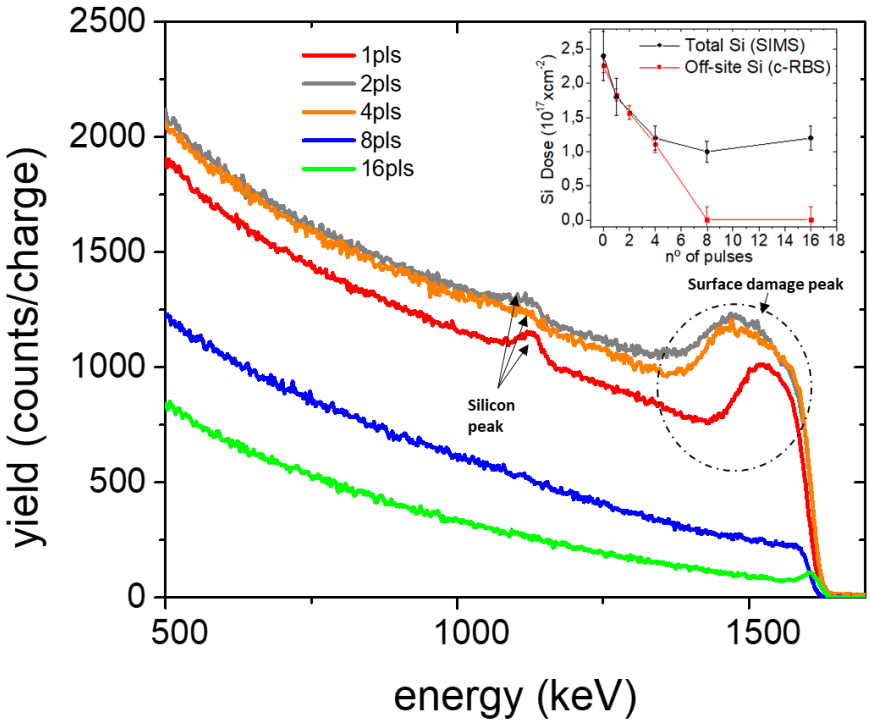

Fig. 3: c-RBS spectra for samples annealed at an energy fluence of 950 mJ/cm^2 and different number of pulses –pls in the graph- from 1 to 16 (1, 2, 4, 8 and 16 pulses are represented by red, gray, orange, blue and green lines, respectively). Inset: comparison of total Si dose (cm^{-2}) estimated by SIMS (black) and off-site Si dose c-RBS (red) versus number of pulses.

An improved crystalline quality when the number of pulses is increased is confirmed as well from HR-XRD measurements (Fig. 4). The signal at higher angles detected for 8 and 16 pulses, indicates a crystalline layer whose out-of-plane lattice parameter is smaller than Ge, which is compatible with the formation of a crystalline silicon germanium (SiGe) alloy. In contrast, in the case of one single pulse, this crystalline phase is not detected and only the Ge substrate peak appears with a slightly higher FWHM, indicative of a defective or disordered layer in very good agreement with c-RBS. Moreover, the continuous range of perpendicular lattice parameters observed for the sample irradiated with 8 pulses -as compared with the well-defined emerging peak in the

sample with 16 pulses- could be explained by a higher concentration gradient for the 8 pulses' sample, as compared with the more uniform Si concentration as a function of depth in the 16 pulses' sample, in agreement with SIMS Si concentration depth profiles reported in Fig. 2. On the other hand, this could be also related with a better crystalline quality for the sample irradiated with 16 pulses (in agreement with c-RBS, Fig. 3).

To determine the composition of the theoretical SiGe alloy detected by HRXRD, Vegard's law [37] has been applied to the 16 pulses' sample, obtaining a Si concentration between 6 and 11%, depending on the degree of relaxation of the material assumed. It should be mentioned that this percentage of Si, although estimated from different characterization techniques, should be taken cautiously as the presence of C could affect the lattice strain of SiGe alloys leading to deviations from Vegard's law [38]. However, the fact that the total percentage of Si with respect to C and Ge estimated from SIMS is around 4% up to a depth of 450 nm where it starts decreasing, suggests that the SiGe layer in the 16 pulses' sample is pseudomorphous with respect to the Ge substrates.

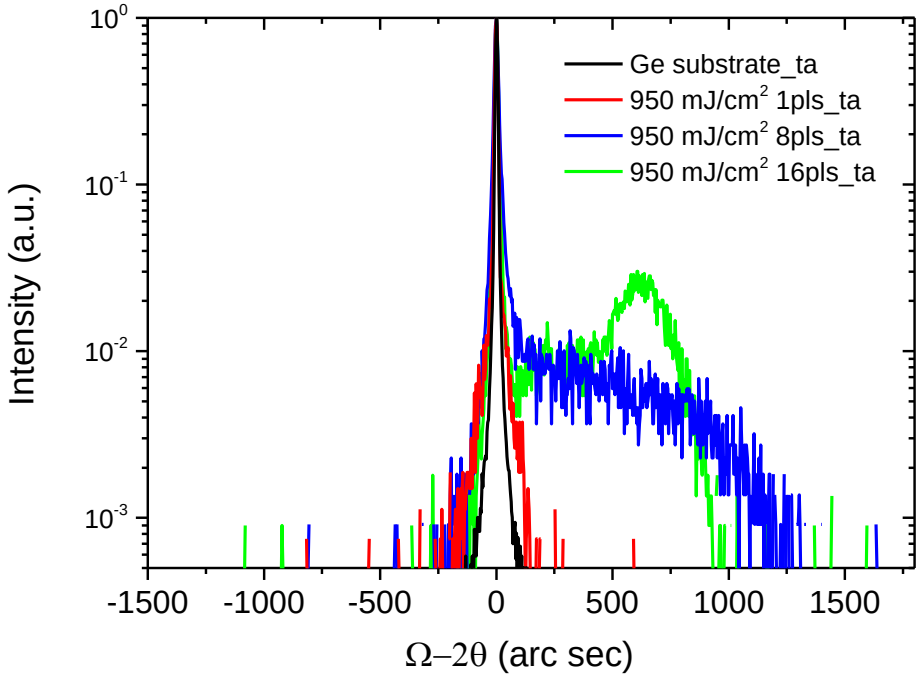

Fig. 4 Ω-2Θ scan of samples annealed at an energy fluence of 950 mJ/cm^2 and different number of pulses –pls in the graph- (1-8-16 pls -in red, blue and green curve, respectively-) and Ge substrate (black curve) as a reference.

Finally, to better understand the qualitative enhancement in the crystalline quality of the laser irradiated samples when the number of pulses is increased, as observed by c-RBS and HRXRD, fig. 5 shows the crystalline structure of two different samples -950 J/cm^2 1 and 8 pulses- analyzed by TEM.

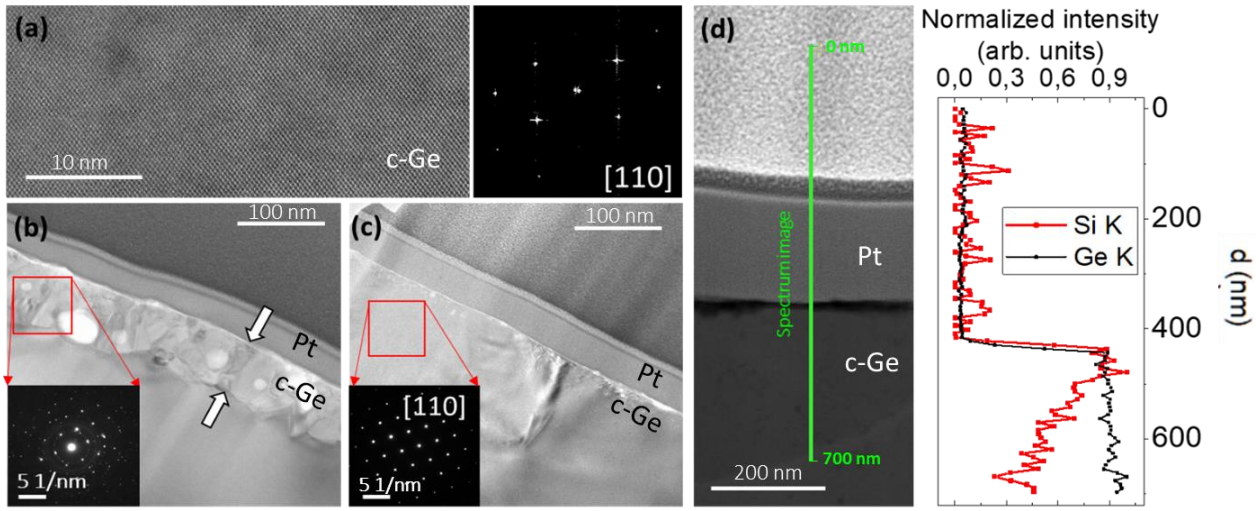

Fig. 5 TEM images of irradiated substrates: (a) Left side: HAADF image of an irradiated substrate after 8 pulses at a depth of around 300 nm from the surface. Right side: high resolution transmission electron microscopy (HR-TEM) image of the crystalline substrate with the FFT of the same image showing the [110] c-Ge zone axis. (b) and (c) after 1 and 8 pulses, respectively, at the surface. (d) Normalized intensity of EDS signals of Si and Ge K edges from the spectrum image indicated by the green line in (d).

The high quality of the Ge substrates is confirmed for 1 and 8 pulses irradiated Ge with the 8 pulses irradiated substrate shown in fig. 5 (a), where a high-resolution high angle annular dark field (HAADF) STEM image exhibits the monocrystallinity of c-Ge in the [110] zone axis observed also in the fast Fourier transform (FFT). However, 1 pulse and 8 pulses substrates present remarkable differences in the vicinity of the surface. 1 pulse irradiated sample reveals a polycrystalline region near the surface, i.e. around the first 250 nm, indicated by white arrows. In addition to the evidence shown by the real space TEM image from fig. 5(b), the disks shown at the diffraction pattern of the red square region confirm the presence of several crystals orientations. This result is at variance with the 8 pulses substrate –fig. 5 (c)-, that is monocrystalline with some defects up to the surface as can be observed by the [110] diffraction pattern of the red square zone. The polycrystalline nature of the 1 pulse sample is in very good agreement with the damage peak observed by c-RBS and the defective layer deduced from HRXRD. Furthermore, the qualitative enhancement in crystalline quality observed by c-RBS and HRXRD as the number of pulses increases, is also confirmed as the near-surface region becomes monocrystalline for the 8 pulses sample.

Concerning the Si diffusion into Ge substrate, fig. 5 (d) displays a high resolution HAADF image of the 8 pulses irradiated sample where the green line indicates the region of the EDS spectrum image with the normalized intensity signals of Si and Ge K edges presented aside. Once again Si diffusion into the Ge substrate is confirmed, having its maximum intensity at a depth of more than 300 nm. This result is consistent with the findings of the SIMS measurement for the 8 pulses irradiated sample, where the Si and P diffuse very similarly and up to 800 nm depth. In EDS spectrum images, the P K signal has not been considering for extra caution, because of the overlapping of P K edge with Pt K edge coming from the surface of the substrate. Neither C has been considered in

the EDS analysis, since C is commonly observed as a contaminant that arises from the sample preparation process and from the environment. This C contamination prevents us from quantifying the C concentration using TEM analytical techniques [39].

4.2. ELECTRICAL CHARACTERIZATION

Further considerations of utmost importance for the development of Ge-based devices arise from fig. 6, where the electrical performance of the resulting P-doped Ge samples is evaluated in terms of sheet resistance R_{SH} (Ω/□), sheet carrier density n_s (also known as active carrier dose) (cm^{-2}) and Hall mobility μ_H ($cm^2 \cdot V^{-1} \cdot s^{-1}$). As it can be seen, very high R_{SH} (> 1000 Ω/□) and n_s (close to $1x10^{13}$ cm^{-2}) is obtained up to 4 pulses, independently of the energy fluence used, suggesting a very low electric activation. However, above 4 pulses, there is a threshold, from which the electrical activation drastically improves, obtaining a much higher electrically-activated P dose (>$1x10^{14}$ cm^{-2}) for the samples irradiated with 8 and 16 pulses, close to the chemical dose estimated by SIMS also represented in fig. 6 with a black star. This phenomenon could be related likewise with the major improvement in crystalline quality observed for samples irradiated above 4 pulses too.

Correspondingly, μ_H shows an initial increase up to 4 pulses, likely due to the gradual reduction of aforementioned defectiveness. Thereafter, it reduces for a large number of pulses, as expected for emerging of ionized impurity scattering, namely from electrically active donors. Indeed, the more heavily Ge is doped, the higher is the probability that carriers will collide with ionized P in a given time, and the smaller the mean free time between collisions, and μ_H reduces accordingly. In fact, the sample irradiated with 750 mJ/cm^2, which has a lower active carrier dose (as shown in panel b), shows a higher mobility as compared with 950 mJ/cm^2 for all pulse conditions.

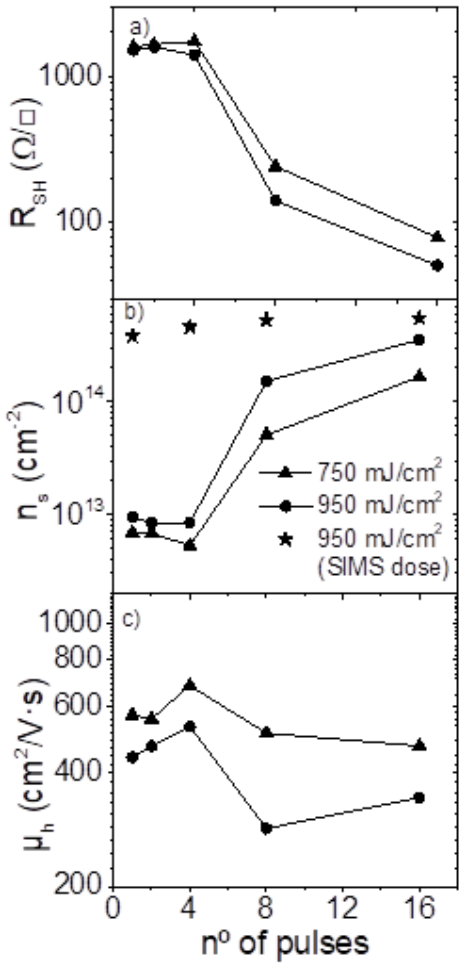

Fig. 6 Sheet resistance (Ω/□), active dose (cm^{-2}) and hall mobility ($cm^2/V{\cdot}s$) of laser-annealed samples at two different energy fluences (750 and 950 mJ/cm^2 -represented by triangles and circles, respectively-) as a function of the number of pulses (1-16 pulses). The chemical dose (cm^{-2}) calculated from SIMS (star symbol) is represented together with the active dose (cm^{-2}) from Hall measurements for comparison purposes.

To better understand the level of activation of P at the surface, which can influence ohmic contact formation, the average P active surface concentration has been calculated by combining the results obtained from Hall and SIMS as explained in the section "Material and Methods". The results of such calculations are reported in fig. 7, where mobility values between 340 and 530 $cm^2/V{\cdot}s$ are found for samples irradiated with 950 mJ/cm energy fluence, which corresponds to electron active concentration in Ge in the range of 10^{17}-10^{19}, consistently with the chemical concentration measured by SIMS. Our measurements indicate that in the highly defective samples (1 pulse) the dependence of the mobility on the free carrier concentration does not follow the one expected for uniformly doped uncompensated germanium -experimentally established by *Fistul et al.* [40] and corroborated in our last work also for laser-doped Ge[1] [41] - as deduced from fig. 7 (i.e. for an active electron concentration of around $4{\cdot}10^{17}$ cm^{-3} the expected mobility would be 1100 $cm^2V^{-1}s^{-1}$. Instead, the calculated value for 1-pulse irradiated sample is less than the half expected: 440 $cm^2V^{-1}s^{-1}$). An exception to this result occurs in the sample with 16 pulses (of better crystal quality) which approaches the expected trend. This means that the additional scattering of carriers, when less than 16 pulses are given, might be caused by damage (i.e. polycrystalline near-surface), dislocations or charged impurity centers. Influence of Ge substrate can be in principle ruled out as intrinsic wafers which can be considered as an insulating boundary were used (See Material & Methods). Moreover, mobilities in the order of 3660 $cm^2/V{\cdot}s$ are expected for c-Ge high resistivity wafers with carrier concentration 2×10^{13} cm^{-3} [42], far away from the highest mobility in the order of 530 $cm^2/V{\cdot}s$. It should be also mentioned that a slightly lower mobility is expected as compared with pure Ge because of the presence of the 5-11% of Si in Ge.

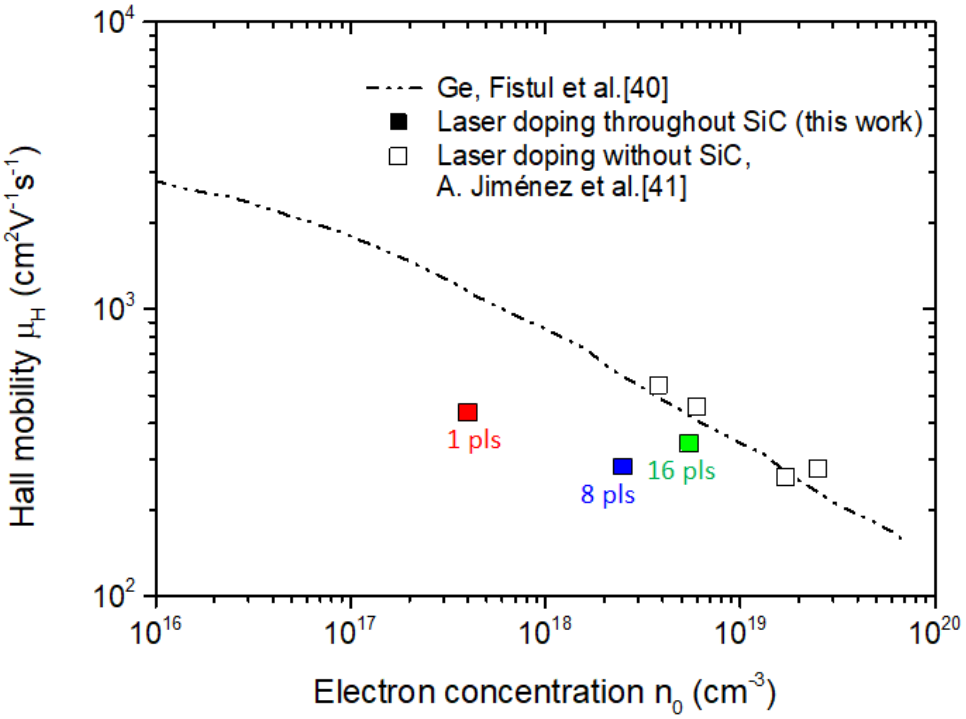

[1]wherein the electron concentration was calculated with the same methodology used in this work and explained in the section "Material and Methods"

Fig. 7. Hall mobility as a function of electron concentration in c-Ge. Filled symbols represents the laser doping approach based on SoD and PLM throughout SiC developed in this work for 950 mJ/cm^2 for different number of pulses –pls in the graph- (1-8-16 pls -in red, blue and green, respectively-) with empty symbols representing the laser doping approach based on SoD sources without SiC [41]

Once that highly doped regions of relatively good crystalline quality have been demonstrated under certain laser conditions, a first proof-of-concept has been done to validate our technology for electron-selective contacts for p-type Ge by fabricating a diode. The laser condition chosen for n-type doping has been 950 mJ/cm^2 and 16 pulses since it is the one that resulted in the highest level of electrical activation and crystalline quality between the range of studied laser conditions. Contact formation is done by using aluminium and Pd/Ti/Pd/Ag for p- and n-type contacts, respectively, without any additional high temperature step. Figure 8 shows the results from the dark IV curve characteristics of the fabricated Ge diode, with the results obtained for the saturation current density (J_{01}), the ideality factor (n_1) and series and shunt resistances (R_s and R_{sh}) resulting from the fitting of the experimental data to a one diode model, commonly used to model PV devices [43]. Firstly, we can see that the obtained series resistance is 8.66 mΩ·cm^2 which can be considered quite low. Despite further research is needed to identify how every element of the device contributes to it, this result demonstrates that the laser doped n^+ region and its metal contact permits the electron transport through them with low ohmic losses, i.e. the contact resistivity is low. Secondly, the very low shunt resistance could be explained by the formation of microcracks on the laser-doped region, which can provide a path for the metal to be in direct contact with the p-type Ge substrate inducing shunts [44]. Finally, forward current mechanism is dominated by an exponential trend with ideality factor 1.69 and fairly high saturation current density. The relative high ideality factor value indicates that current is based on recombination in the space charge region where significant recombination centers may be left. Despite large saturation currents are expected in Ge due to its low band gap, the obtained result is worse than the best experimental results obtained in the range of 1E-05 - 1E-06 A/cm^2 for ideal diffusion currents, i.e. ideality factor equal to 1 [45]. However, it must be noticed that only a small fraction of the surface will be processed in final devices, most probably resulting in a better surface passivation (lower saturation current) and a higher shunt resistance. The former is based on the replacement of the laser processed regions by dielectric passivated surfaces where an excellent surface recombination velocity as low as 15 cm/s has been measured (see “Material and methods”); while the latter may simply be improved by the much smaller laser processed area. The detailed calculation of the saturation current density and shunt resistance in such devices needs an optimization of their geometry which is beyond the scope of this paper. However, significant improvement on both parameters is expected taking into account that typically a 1-5% of the area is laser processed in finished devices [46], [47]. Besides, different thicknesses of the dielectric layer a-Si_xC_{1-x}:H could be also explored, as they could affect the optimum energy fluence conditions. It is expected that the use of a lower energy fluence results in a lower melting volume of Ge. A large volume can hamper a proper re-align of the crystal during the fast cooling and re-solidification that could result in the formation of laser-induced defects [44]. Finally other metallization

techniques should be considered, as for instance photoplating, which has demonstrated to be certainly effective for shunting prevention in laser-doped Si solar cells thanks to its selectivity as proven by *Hameiri et al.* [48].

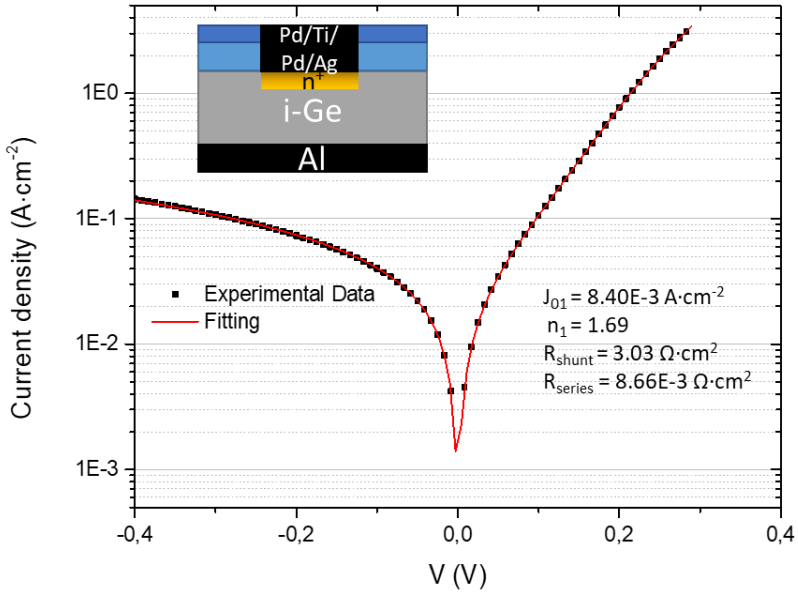

Fig. 8. Diode fabricated with PLM based on SoD throughout an aSi_xC_{1-x}:H layer with laser condition: 950 mJ/cm^2 and 16 pulses. Table: Electrical performance of the diode fabricated with PLM based on SoD throughout SiC stack with laser condition: 950 mJ/cm^2 and 16 pulses.

5. CONCLUSIONS

We have successfully demonstrated a method for electron selective contact formation on p-type Ge based on PLM of P-SoD through an insulating SiC stack, as a step towards the manufacturing of low-cost Ge-IBC cells. The major advantage of this method is that it allows simultaneous opening of the insulating layer and creation of a heavily doped region underneath reducing the number of photolithographic steps, eventually enabling a low-cost and scalable manufacturing process.

The impact of the energy fluence (750-950 mJ/cm^2) and the number of pulses (1-16) on the chemical, electrical, structural and morphological characteristics has been experimentally studied. High electrically-activated P dose (>1x10^{14} cm^{-2}) corresponding to a level of dopant active concentration around 10^{19} cm^{-3} has been achieved, with a strong dependency of the level of activation on the number of pulses and a weaker dependency on the energy fluence. The results indicate that at least 8 pulses are needed for reaching high donor activation with the best results obtained for 16 pulses, case in which mobility approaches the one expected for uniformly doped uncompensated Ge. Similarly, crystalline quality is improved at over 8 pulses, as deduced from c-RBS and HRXRD measurements, with the higher level of crystallinity being also obtained for 16 pulses. This agrees with TEM measurements where a SiGe polycrystalline alloy near the surface is detected in the case of using 1 single pulse in contrast to a monocrystalline

SiGe alloy in the case of using 8 pulses. This SiGe layer has been unintentionally formed as a consequence of the diffusion of Si from the phase separation of the insulating SiC stack during laser irradiation.

A first proof-of-concept diode has been fabricated using the sample irradiated with 16-pulses and 950 mJ/cm^2 demonstrating rectifying behavior, although a very low shunt resistance and relatively high saturation currents are obtained. Punctual contact formation is expected to drastically improve the surface passivation, and thus, improve the diode characteristics. Different SiC thicknesses and laser energy fluences should be also explored to minimize the risk of shunting through the SiC electrically insulating layer.

Acknowledgments

A. Jiménez acknowledges 'Programa de Ayudas a la Investigación en Energía y Medio Ambiente 2019-2020 y 2020-2021' from Fundación Iberdrola, 'Programa Propio I+D+i para contratos predoctorales' from Universidad Politécnica de Madrid and 'Programa de Ayudas para el fomento de la formación y la internalización de doctorandos' from Consejo Social Universidad Politécnica de Madrid. A. Jiménez and A. Datas acknowledges the Spanish Minister for Science and the Agencia Estatal de Investigación for the funding provided in the Project TERMOCELL (ENE2017-86683-R - MINECO/AEI/FEDER, UE) with the support of FEDER funds and the Universidad Politécnica de Madrid, the Regional Government of Madrid for the project ANDREA funded in the "programa de apoyo a la realización de Proyectos de I+D para jóvenes investigadores 2019" and the funding under project GEPTV (PID2020-115719RB-C22) funded by MCIN/ AEI /10.13039/501100011033. This work has been partially funded from the University of Padova through the grant UNIPD-ISR 2017 'SENSITISE'. Luca Bacci and Nicola Argiolas (University of Padova) are acknowledged for their precious technical assistance. Chiara Carraro (University of Padova) is acknowledged for helping discussions and technical assistance in the lab. Isidro Martín and Gema López acknowledge the funding under project GETPV (PID2020-115719RB-C21) funded by MCIN/ AEI /10.13039/501100011033. I.García acknowledges AEI's funding through project RTI2018-094291-B-I00 Y. K. Ryu and J. Martinez would like to acknowledge ICTS Micronanofabs.

REFERENCES

[1] L. M. Fraas, W. E. Daniels, J. Avery, J. E. Samaras, and J. B. Keyes, 'Shingle circuits for thermophotovoltaic systems'

[2] H. Hayden *et al.*, 'CPV semi-dense array design for dish and tower collectors', San Diego, California, USA, Oct. 2012, p. 84680I. doi: 10.1117/12.930054.

[3] G. Kinsey *et al.*, 'Multijunction Solar Cells for Dense-Array Concentrators', in *2006 IEEE 4th World Conference on Photovoltaic Energy Conference*, Waikoloa, HI, 2006, pp. 625–627. doi: 10.1109/WCPEC.2006.279532.

[4] A. Salemi, M. Eccher, A. Miotello, and R. S. Brusa, ‘Dense array connections for photovoltaic systems in concentration’, *Prog. Photovolt. Res. Appl.*, vol. 19, no. 4, pp. 379–390, Jun. 2011, doi: 10.1002/pip.1040.

[5] F.-L. Siaw and K.-K. Chong, ‘A Systematic Method of Interconnection Optimization for Dense-Array Concentrator Photovoltaic System’, *Sci. World J.*, vol. 2013, pp. 1–11, 2013, doi: 10.1155/2013/275169.

[6] F.-L. Siaw, K.-K. Chong, and C.-W. Wong, ‘A comprehensive study of dense-array concentrator photovoltaic system using non-imaging planar concentrator’, *Renew. Energy*, vol. 62, pp. 542–555, Feb. 2014, doi: 10.1016/j.renene.2013.08.014.

[7] A. Datas and P. G. Linares, ‘Monolithic interconnected modules (MIM) for high irradiance photovoltaic energy conversion: A comprehensive review’, *Renew. Sustain. Energy Rev.*, vol. 73, pp. 477–495, Jun. 2017, doi: 10.1016/j.rser.2017.01.071.

[8] G. Lu, J. Wang, Z. Qian, and W. Shen, ‘Development of back-junction back-contact silicon solar cells based on industrial processes: Back-junction back-contact silicon solar cells’, *Prog. Photovolt. Res. Appl.*, vol. 25, no. 6, pp. 441–451, Jun. 2017, doi: 10.1002/pip.2881.

[9] G. López *et al.*, ‘Base contacts and selective emitters processed by laser doping technique for p-type IBC c-Si solar cells’, *Energy Procedia*, vol. 77, pp. 752–758, Aug. 2015, doi: 10.1016/j.egypro.2015.07.106.

[10] G. López, P. R. Ortega, I. Martín, C. Voz, A. Orpella, and R. Alcubilla, ‘“Cold” Process for IBC c-Si Solar Cells Fabrication’, *Energy Procedia*, vol. 92, pp. 652–660, Aug. 2016, doi: 10.1016/j.egypro.2016.07.032.

[11] M. D. Lammert and R. J. Schwartz, ‘The interdigitated back contact solar cell: A silicon solar cell for use in concentrated sunlight’, *IEEE Trans. Electron Devices*, vol. 24, no. 4, pp. 337–342, Apr. 1977, doi: 10.1109/T-ED.1977.18738.

[12] P. Verlinden, ‘Interdigitated Back Contact Solar Cells’, in *Photovoltaic Solar Energy*, A. Reinders, P. Verlinden, W. van Sark, and A. Freundlich, Eds. Chichester, UK: John Wiley & Sons, Ltd, 2017, pp. 92–103. doi: 10.1002/9781118927496.ch10.

[13] T. Burger, C. Sempere, B. Roy-Layinde, and A. Lenert, ‘Present Efficiencies and Future Opportunities in Thermophotovoltaics’, *Joule*, vol. 4, no. 8, pp. 1660–1680, Aug. 2020, doi: 10.1016/j.joule.2020.06.021.

[14] J. Fernández, ‘Development of Crystalline Germanium for Thermophotovoltaics and High Efficiency Multi-Junction Solar Cells’, Fraunhofer, Freiburg (Germany), 2010. [Online]. Available: http://nbn-resolving.de/urn:nbn:de:bsz:352-203218

[15] J. Melskens *et al.*, ‘Concepts and prospects of passivating contacts for crystalline silicon solar cells’, in *2015 IEEE 42nd Photovoltaic Specialist Conference (PVSC)*, New Orleans, LA, Jun. 2015, pp. 1–6. doi: 10.1109/PVSC.2015.7355646.

[16] E. U. Onyegam *et al.*, 'Exfoliated thin, flexible monocrystalline germanium heterojunction solar cells', in *2012 38th IEEE Photovoltaic Specialists Conference*, Austin, TX, USA, Jun. 2012, pp. 002578–002582. doi: 10.1109/PVSC.2012.6318122.

[17] T. Kaneko and M. Kondo, 'High Open-Circuit Voltage and Its Low Temperature Coefficient in Crystalline Germanium Solar Cells Using a Heterojunction Structure with a Hydrogenated Amorphous Silicon Thin Layer', *Jpn. J. Appl. Phys.*, vol. 50, p. 120204, Nov. 2011, doi: 10.1143/JJAP.50.120204.

[18] B. Hekmatshoar, D. Shahrjerdi, M. Hopstaken, K. Fogel, and D. K. Sadana, 'High-efficiency heterojunction solar cells on crystalline germanium substrates', *Appl. Phys. Lett.*, vol. 101, no. 3, p. 032102, Jul. 2012, doi: 10.1063/1.4737166.

[19] S. Nakano, Y. Takeuchi, T. Kaneko, and M. Kondo, 'Influence of surface treatments on crystalline germanium heterojunction solar cell characteristics', *J. Non-Cryst. Solids*, vol. 358, no. 17, pp. 2249–2252, Sep. 2012, doi: 10.1016/j.jnoncrysol.2011.12.045.

[20] N. E. Posthuma, 'Development Of Low Cost Germanium Photovoltaic Cells For Application In TPV Using Spin On Diffusants', in *AIP Conference Proceedings*, Freiburg (Germany), 2004, vol. 738, pp. 337–344. doi: 10.1063/1.1841911.

[21] J. van der Heide, N. E. Posthuma, G. Flamand, W. Geens, and J. Poortmans, 'Cost-efficient thermophotovoltaic cells based on germanium substrates', *Sol. Energy Mater. Sol. Cells*, vol. 93, no. 10, pp. 1810–1816, Oct. 2009, doi: 10.1016/j.solmat.2009.06.017.

[22] J. W. Baek, J. Shim, and J.-H. Park, 'Characteristics of Germanium n+/p junctions formed by phosphorus diffusion from on indium-gallium-phosphide layer', *Curr. Appl. Phys.*, vol. 15, no. 7, pp. 765–769, Jul. 2015, doi: 10.1016/j.cap.2015.04.040.

[23] K. S. Petrovna, I. Anfimov, and S. Yurchuk, 'Phosphorus and Gallium Diffusion in Ge Sublayer of In0.01Ga0.99As/In0.56Ga0.44P/Ge Heterostructures', in *Advanced Material and Device Applications with Germanium*, S. Lee, Ed. InTech, 2018. doi: 10.5772/intechopen.78347.

[24] B. Bouzazi, A. Jaouad, A. Turala, R. Arès, S. Fafard, and V. Aimez, 'InGaP/Ge and GaAs/Ge double-junction solar cells for thermal-CPV hybrid energy systems', Puertollano, Spain, 2018, p. 110001. doi: 10.1063/1.5053549.

[25] A. S. Gudovskikh, K. S. Zelentsov, N. A. Kalyuzhnyy, V. M. Lantratov, S. A. Mintairov, and J. P. Kleider, 'Characterization of GaInP/Ge heterostructure solar cells by capacitance measurements at forward bias under illumination', *Energy Procedia*, vol. 3, pp. 76–83, 2011, doi: 10.1016/j.egypro.2011.01.013.

[26] T. Nagashima, K. Hokoi, K. Okumura, and M. Yamaguchi, 'Surface Passivation for Germanium and Silicon Back Contact Type Photovoltaic Cells', in *2006 IEEE 4th World Conference on Photovoltaic Energy Conference*, Waikoloa, HI, 2006, pp. 655–658. doi: 10.1109/WCPEC.2006.279540.

[27] R. Duffy, E. Napolitani, and F. Cristiano, 'Materials science issues related to the fabrication of highly doped junctions by laser annealing of Group IV semiconductors', in *Laser Annealing Processes in Semiconductor Technology*, Elsevier, 2021, pp. 175–250. doi: 10.1016/B978-0-12-820255-5.00007-6.

[28] J. Fernández, F. Dimroth, E. Oliva, M. Hermle, and A. W. Bett, 'Back-surface Optimization of Germanium TPV Cells', in *AIP Conference Proceedings*, Madrid (Spain), 2007, vol. 890, pp. 190–197. doi: 10.1063/1.2711736.

[29] S. R. Wenham, M. Heights, and M. A. Green, 'Self aligning method for forming a selective emitter and metallization in a solar cell', US 6,429,037 B1

[30] I. Martin, A. Alcaniz, A. Jimenez, G. Lopez, C. del Canizo, and A. Datas, 'Application of Quasi-Steady-State Photoconductance Technique to Lifetime Measurements on Crystalline Germanium Substrates', *IEEE J. Photovolt.*, pp. 1–8, 2020, doi: 10.1109/JPHOTOV.2020.2981839.

[31] V. Boldrini *et al.*, 'Optimal process parameters for phosphorus spin-on-doping of germanium', *Appl. Surf. Sci.*, vol. 392, pp. 1173–1180, Jan. 2017, doi: 10.1016/j.apsusc.2016.09.134.

[32] M. Gavelle *et al.*, 'Detection of Cs2Ge+ clusters for the quantification of germanium atoms by secondary ion mass spectrometry: Application to the characterization of Si1−xGex layers (0⩽x⩽1) and germanium diffusion in silicon', *J. Appl. Phys.*, vol. 102, no. 7, p. 074904, Oct. 2007, doi: 10.1063/1.2786037.

[33] F. Sánchez-Almazán *et al.*, 'Matrix effects in SIMS depth profiles of SiGe relaxed buffer layers', *Appl. Surf. Sci.*, vol. 231–232, pp. 704–707, Jun. 2004, doi: 10.1016/j.apsusc.2004.03.193.

[34] J. F. Ziegler and J. P. Biersack, 'The Stopping and Range of Ions in Matter', in *Treatise on Heavy-Ion Science*, D. A. Bromley, Ed. Boston, MA: Springer US, 1985, pp. 93–129. doi: 10.1007/978-1-4615-8103-1_3.

[35] G. Impellizzeri *et al.*, 'Aluminium Implantation in Germanium: Uphill Diffusion, Electrical Activation, and Trapping', *Appl. Phys. Express*, vol. 5, no. 2, p. 021301, Jan. 2012, doi: 10.1143/APEX.5.021301.

[36] C. Claeys and E. Simoen, *Germanium-based technologies: From materials to devices*. 2007.

[37] A. R. Denton and N. W. Ashcroft, 'Vegard's law', *Phys. Rev. A*, vol. 43, no. 6, pp. 3161–3164, Mar. 1991, doi: 10.1103/PhysRevA.43.3161.

[38] P. C. Kelires, 'Theory of bonding, strain, and segregation in germanium-carbon alloys', *Phys. Rev. B*, vol. 60, no. 15, pp. 10837–10844, Oct. 1999, doi: 10.1103/PhysRevB.60.10837.

[39] D. I. Garcia-Gutierrez, M. José-Yacamán, S. Lu, D. Q. Kelly, and S. K. Banerjee, 'Carbon segregation as a strain relaxation mechanism in thin germanium-carbon layers

deposited directly on silicon', *J. Appl. Phys.*, vol. 100, no. 4, p. 044323, Aug. 2006, doi: 10.1063/1.2336305.

[40] V. I. Fistul, M. I. Iglitsyn, and E. M. Omelyanovskii, 'Mobility of electrons in germanium strongly doped with arsenic', vol. 4, pp. 784–785, 1962.

[41] A. Jiménez *et al.*, 'N-type doping of Ge by P spin on dopant and pulsed laser melting', *Semicond. Sci. Technol.*, vol. 35, no. 6, p. 065002, Jun. 2020, doi: 10.1088/1361-6641/ab7bed.

[42] C. Carraro *et al.*, 'N-type heavy doping with ultralow resistivity in Ge by Sb deposition and pulsed laser melting', *Appl. Surf. Sci.*, vol. 509, p. 145229, Apr. 2020, doi: 10.1016/j.apsusc.2019.145229.

[43] A. Hovinen, 'Fitting of the solar cell IV-curve to the two diode model', *Phys. Scr.*, vol. T54, pp. 175–176, Jan. 1994, doi: 10.1088/0031-8949/1994/T54/043.

[44] B. Tjahjono, 'Laser doped selective emitter solar cells', University of New South Wales, Sydney, 2010.

[45] T. Bauer, *Thermophotovoltaics: Basic Principles and Critical Aspects of System Design*. Berlin, Heidelberg: Springer Berlin Heidelberg, 2011. doi: 10.1007/978-3-642-19965-3.

[46] P. Ortega *et al.*, 'Fully low temperature interdigitated back-contacted c-Si(n) solar cells based on laser-doping from dielectric stacks', *Sol. Energy Mater. Sol. Cells*, vol. 169, pp. 107–112, Sep. 2017, doi: 10.1016/j.solmat.2017.05.017.

[47] M. Ernst *et al.*, 'Fabrication of a 22.8% Efficient Back Contact Solar Cell With Localized Laser-Doping', *Phys. Status Solidi A*, vol. 214, no. 11, p. 1700318, Nov. 2017, doi: 10.1002/pssa.201700318.

[48] Z. Hameiri, L. Mai, and S. R. Wenham, 'Advantages of photoplating for laser doped solar cells: Advantages of photoplating', *Prog. Photovolt. Res. Appl.*, vol. 19, no. 5, pp. 511–516, Aug. 2011, doi: 10.1002/pip.1072.